Quantum-orbit theory of low-energy above-threshold ionization on and off axis

W. Becker[1,*] and D. B. Milošević[1,2,3]

[1]*Max-Born-Institut, Max-Born-Str. 2a, 12489 Berlin, Germany*
[2]*Faculty of Science, University of Sarajevo, Zmaja od Bosne 35, 71000 Sarajevo, Bosnia and Herzegovina*
[3]*Academy of Sciences and Arts of Bosnia and Herzegovina, Bistrik 7, 71000 Sarajevo, Bosnia and Herzegovina*
**Corresponding author: wbecker@mbi-berlin.de*

Received February 23, 2015; accepted May 7, 2015; posted online June 26, 2015

Intense-laser-induced above-threshold ionization of a bound electron into continuum states with low energy is investigated in the context of the strong-field approximation that allows for one act of rescattering of the revisiting electron. The quantum orbits for forward and backward scattering are evaluated and generalized to arbitrary scattering angles. The velocity map of the liberated electron exhibits the well-known low-energy structure as well as other features off the polarization axis.

OCIS codes: 020.2649, 190.4180, 270.4180, 270.6620, 320.7110.
doi: 10.3788/COL201513.070006.

Recollisions of the liberated electron with its parent ion are responsible for the most spectacular and important effects of strong-field physics, such as high-order harmonic generation and high-order above-threshold ionization (ATI)[1]. In the recollision, the electron can scatter in any direction[2]. In ATI, the interest has focused on backscattering, since this is what generates high energies and the ATI plateau[3]. If the electron scatters in the forward direction, its final energy is comparatively low and it has to compete with other pathways to low energy, the so-called direct electrons, which do not rescatter at all and have been expected to be dominant. Hence, for low electron energies, it has been tacitly assumed that forward scattering, and rescattering in general, make a negligible contribution. However, this is not necessarily true because, for Coulomb scattering, the forward-scattering (FS) amplitude is very large, actually divergent. Indeed, Coulomb forward scattering was proposed[4] and is now widely accepted as the origin of the so-called low-energy structure (LES)[5,6] in ATI.

In this Letter, we will consider forward and backward scattering as well as rescattering by an arbitrary angle into states with low final energy. We will employ the quantum-mechanical quantum-orbit theory, which is built on the improved strong-field approximation (ISFA)[7–9]. The ISFA considers rescattering in first-order Born approximation; in other words, in the Born series the Coulomb potential acts on the electron at most once after its liberation via tunneling. However, the ISFA can be generalized to the low-frequency approximation (LFA), which incorporates potential scattering in the absence of the laser field to arbitrary order[10–13]. It came as a surprise that already the ISFA, even though it is only of first order in the scattering potential, accounts for the LES structures[14].

An outline of this Letter is as follows. We start by introducing the ATI amplitude and its quantum-orbit expansion in the case of a linearly polarized, infinitely long, flat laser pulse. We define forward and backscattering contributions and compare their relative significance for given final energy. We consider the angular dependence of the ATI spectra and derive the angular dependence of the various cutoffs from the classical simple-man model. Finally, we present momentum-plane spectra for various quantum orbits of FS and backward-scattering (BS), with special emphasis on the low-energy region. The atomic system of units ($\hbar = |e| = m = 4\pi\varepsilon_0 = 1$) is used throughout the Letter.

The rescattering T-matrix element for ionization from a bound state ψ_i, having the ionization energy $I_p = -E_i$, to a final state of an electron with an asymptotic momentum $\mathbf{p}$, in the saddle-point approximation is given by[8,15–17]

$$T^R_{\mathbf{p}i} \propto \sum_s \Delta_s^{-1/2} \mathcal{M}_{\mathbf{p}\mathbf{k}_{\rm st}}(t_s) \mathcal{M}_{\mathbf{k}_{\rm st} i}(t_{0s}) e^{iS_s}. \tag{1}$$

The corresponding differential ionization rate is given by $w_{\mathbf{p}i} = 2\pi p |T^R_{\mathbf{p}i}|^2$. The sum over s is the sum over the relevant solutions of the system of the two saddle-point equations for the ionization time t_{0s} and the rescattering time t_s

$$\frac{1}{2}[\mathbf{k}_{\rm st} + \mathbf{A}(t_0)]^2 = -I_p, \tag{2}$$

$$\frac{1}{2}[\mathbf{k}_{\rm st} + \mathbf{A}(t)]^2 = \frac{1}{2}[\mathbf{p} + \mathbf{A}(t)]^2, \tag{3}$$

where $\mathbf{k}_{\rm st} = \int_{t_0}^{t} \mathrm{d}t' \mathbf{A}(t')/(t_0 - t)$ is the stationary momentum. In length gauge and dipole approximation, the ionization matrix element is $\mathcal{M}_{\mathbf{k}_{\rm st} i}(t_0) = \langle \mathbf{k}_{\rm st} + \mathbf{A}(t_0) | \mathbf{r} \cdot \mathbf{E}(t_0) | \psi_i \rangle$, where $\mathbf{E}(t)$ is the electric-field vector. For a monochromatic linearly polarized field with period $T = 2\pi/\omega$ (in the direction determined by the unit vector $\hat{\mathbf{e}} = \hat{\mathbf{x}}$), we take $\mathbf{E}(t) = \hat{\mathbf{e}} E_0 \sin \omega t$. The action in the exponent of Eq. (1) is $S_s \equiv S(t_{0s}, t_s)$, with $S(t_0, t) = \mathbf{p}^2 t/2 + \mathbf{p} \cdot \boldsymbol{\alpha}(t) + \mathbf{k}_{\rm st}^2 (t - t_0)/2 + (U_p + I_p) t_0 + \mathcal{U}_1(t_0)$,

 © 2015 Chinese Optics Letters

$\mathbf{A}(t) = \hat{\mathbf{e}}A_0 \cos \omega t$, $\alpha(t) = \hat{\mathbf{e}}(A_0/\omega) \sin \omega t$, $\mathcal{U}_1(t) = \int^t \mathrm{d}t' \mathbf{A}^2(t')/2 - U_p t$, $U_p = \int_0^T \mathbf{A}^2(\tau)\mathrm{d}\tau/(2T) = A_0^2/4$, and $A_0 = E_0/\omega$. The determinant $\Delta_s \equiv \Delta(t_{0s}, t_s)$ is given by

$$\Delta(t_0, t) = \left[\frac{i(t-t_0)}{2\pi}\right]^3 \left[\left(\frac{\partial^2 S}{\partial t_0 \partial t}\right)^2 - \frac{\partial^2 S}{\partial t_0^2}\frac{\partial^2 S}{\partial t^2}\right]. \quad (4)$$

Finally, the rescattering matrix element in the LFA has the form[10,17]

$$\mathcal{M}^{\mathrm{LFA}}_{\mathbf{pk}_{\mathrm{st}}}(t) = \langle \psi^{(-)}_{\mathbf{p}+\mathbf{A}(t)} | V | \mathbf{k}_{\mathrm{st}} + \mathbf{A}(t) \rangle, \quad (5)$$

where $\psi^{(-)}_{\mathbf{p}}$ is the continuum eigenstate of the Hamiltonian $-\nabla^2/2 + V$ with the atom-specific rescattering potential $V(r)$ modeled by the sum of the Coulomb potential and a short-range potential[10,17]. A more simplified expression for the rescattering matrix element is obtained if the exact scattering state is replaced with a plane wave [this corresponds to the first Born approximation and this approximation we call the ISFA[7]]: $\mathcal{M}^{\mathrm{ISFA}}_{\mathbf{pk}_{\mathrm{st}}} = \langle \mathbf{p} | V_{\mathrm{sh}} | \mathbf{k}_{\mathrm{st}} \rangle$ [the term $\mathbf{A}(t)$ from Eq. (5) has canceled and only the short-range part of the potential V is taken into account since the matrix element for the Coulomb potential is singular, i.e., $\propto (\mathbf{p} - \mathbf{k}_{\mathrm{st}})^{-2}$].

There are two classes of solutions to the system of the saddle-point equations, i.e., Eqs. (2) and (3)[8,16,18]: the BS solutions, which are classified by the multi-index (α, β, m) in Ref. [8], and the FS solutions, which are classified by the double-index $\nu\mu$ in Ref. [18]. For the case when the motion is restricted to the direction of the laser field, i.e., when $\mathbf{k}_{\mathrm{st}} \| \mathbf{A}(t) \| \mathbf{p}$, we speak of BS if in the instantaneous process of elastic rescattering the electron momentum changes its sign, i.e., if $\mathbf{p} + \mathbf{A}(t) = -[\mathbf{k}_{\mathrm{st}} + \mathbf{A}(t)]$. We speak of FS if the velocity remains the same, such that $\mathbf{k}_{\mathrm{st}} = \mathbf{p}$. The latter case is simple, because in this event Eq. (3) is satisfied for all values of t, while Eq. (2) can be solved analytically for t_0[18]. This means that for a fixed value of $\mathbf{p}$ the solution for t_0 is the same for all $\nu\mu$. For emission away from the polarization axis, the system of Eqs. (2) and (3) should be solved for t_0 and t. This task is simplified since we can start from the known solutions along this axis. Therefore, we keep the term FS for such solutions even in this case. On the other hand, the BS solutions $\{t_{0s}, t_s\}$ are different for each $s \equiv (\alpha, \beta, m)$. As we did for the FS solutions, we will continue to refer by BS to the (α, β, m) solution when the momentum moves away from the polarization axis. We shall see that, for fixed laboratory-frame scattering angle θ, at some point an FS solution becomes BS or vice versa.

LESs were observed in experiments with neutral atoms for high laser intensity and long wavelength[5,6]. In terms of the ponderomotive energy U_p the LES appears in the energy region near and below $0.1\,U_p$. We first consider ATI of Ar atoms by a linearly polarized laser field with intensity 2×10^{14} W/cm^2 and wavelength 2000 nm.

In Fig. 1 we compare the spectra of the electron emitted in the laser polarization direction obtained from BS and FS solutions in various approximations. The results

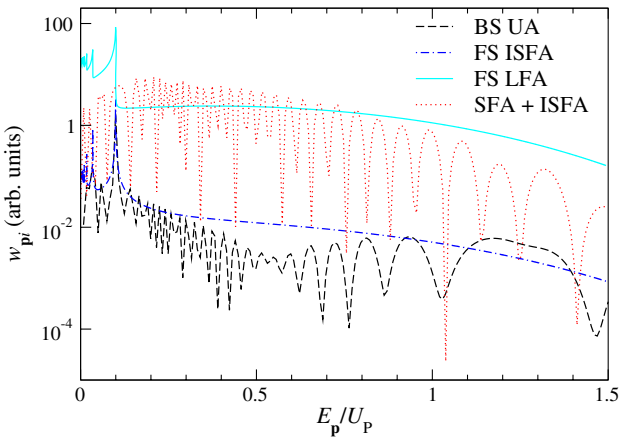

Fig. 1. Differential ionization rates of Ar for the angle $\theta = 0°$ as functions of the electron energy in units of U_p for a linearly polarized laser field with intensity 2×10^{14} W/cm^2 and wavelength 2000 nm ($U_p = 74.7$ eV) for various approximations as explained in the text. The FS LFA spectra obtained using the FS saddle-point solutions within the low-frequency approximation are smooth for energies above $0.1\,U_p$. Below this energy they rise strongly and display the peaks of the classical LES series[18,22].

(SFA + ISFA), which include both the direct electrons (SFA obtained by numerical integration over the ionization time) and the rescattered electrons (ISFA obtained by numerical integration over the ionization and rescattering times) are presented by the red dotted line. This rate is much higher than the one obtained taking only the backscattered electrons within the uniform approximation (BS UA)[10,19–21] or the rate obtained from the forward-scattered electrons within the saddle-point approximation and with the rescattering matrix element taken in the first Born approximation and with a short-range potential (FS ISFA).

In the energy region below $0.1\,U_p$, both the BS UA and the FS ISFA results exhibit sharp peaks at the same positions and with comparable magnitudes. Their common origin are the classical energy cutoffs at $E_{\mathbf{p}} = 8/[(2n+1)^2\pi^2]\,U_p (n = 1, 2, \ldots)$ of the FS solutions[18,22]; cf. Fig. 2(b). These cutoffs cause a sharp maximum of the emission rate, which is due to a near zero of the determinant [Eq. (4)]. The same determinant also multiplies the contributions of the BS orbits in Eq. (1) so that the BS solutions exhibit sharp maxima at the same positions. Indeed, since at these cutoffs the electron returns with zero energy, classically there is no difference between forward- and backscattering. More details can be found in Ref. [16]. However, the rates of both FS (FS ISFA) and BS (BS UA) contributions are far below those of the direct electrons, which are contained in the SFA + ISFA result.

In contrast, the cyan solid line shows the result obtained using the LFA, which includes the exact (with the Coulomb potential included) rescattering matrix element [Eq. (5)] with only the FS saddle-point solutions (FS LFA). We see that in the energy region below $0.1\,U_p$

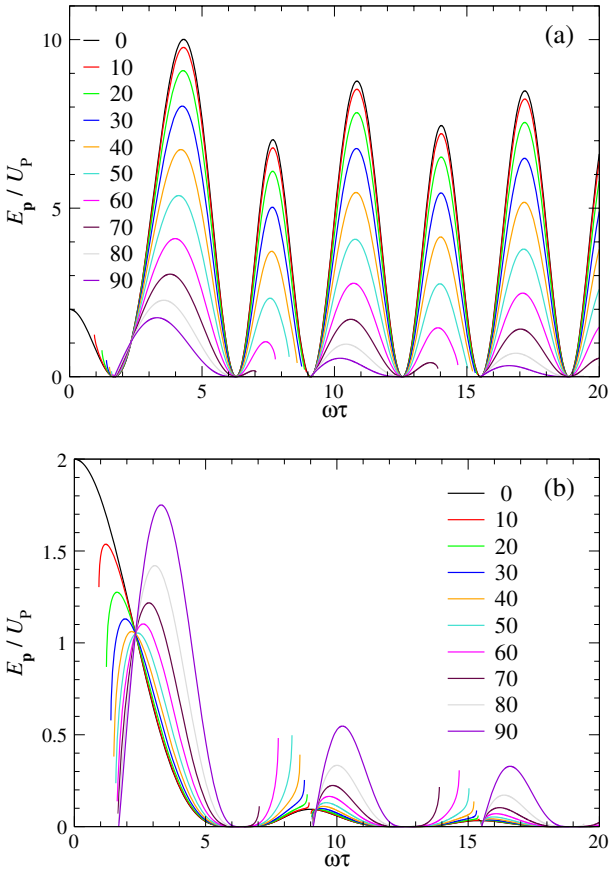

Fig. 2. Classical solutions for the electron energies in units of U_p as a function of the electron travel time (expressed as $\omega\tau$) for backward- (upper panel) and forward- (lower panel) scattered electrons for the final electron emission angle θ between 0° and 90° in steps of 10°, as denoted in the legend.

the corresponding rate is 1 or 2 orders of magnitude larger than the SFA + ISFA rate. In fact, the FS LFA spectra describe the LES as it is observed experimentally: a steep rise for energies below $\approx 0.1\,U_p$ on top of a smooth contribution of low-energy electrons (without the strong oscillations displayed by the other rates).

For energies above about $2\,U_p$ the contributions of the FS solutions quickly become insignificant. High electron energies can only be obtained via backscattering.

In the backscattering case it was possible to give a classical interpretation[23,24] and to determine the classical cutoff as the maximum energy which an electron can have at the detector after backscattering[2]. A similar derivation gives the classical cutoff laws for forward scattering (the LES series of peaks). In this subsection we will consider the general case of an arbitrary electron emission angle θ in the laboratory frame. We will start from the saddle-point Eqs. (2) and (3) in the classical limit when $I_p \to 0$. The stationary momentum is

$$\mathbf{k} = -\mathbf{A}_0 \frac{\sin\omega t - \sin\omega t_0}{\omega\tau}, \qquad \frac{k}{A_0} = -\frac{\sin\sigma\cos\psi}{\sigma}, \quad (6)$$

where we used the relation $\sin\omega t - \sin\omega t_0 = 2\cos\psi\sin\sigma$ and the notation $\sigma = \omega\tau/2$, $\tau = t - t_0$, $\psi = \omega(t + t_0)/2$. The saddle-point equation [Eq. (2)] for $I_p \to 0$ reduces to

$$k + A(t_0) = 0, \quad (7)$$

while the energy-conserving condition [Eq. (3)] at the rescattering time gives

$$[k + A(t)]^2 = [\mathbf{p} + \mathbf{A}(t)]^2. \quad (8)$$

We will also use the relations $\cos\omega t_0 = \cos(\psi - \sigma) = \cos\psi\cos\sigma + \sin\psi\sin\sigma$ and $\cos\omega t = \cos(\psi + \sigma) = \cos\psi\cos\sigma - \sin\psi\sin\sigma$. In this case, Eq. (7) can be rewritten as

$$a\cos\psi - b\sin\psi = 0, \quad (9)$$

where $a = \cos\sigma - \sin\sigma/\sigma$, and $b = -\sin\sigma$. The solutions of Eq. (9) are

$$\sin\psi = sa/\sqrt{a^2 + b^2}, \qquad \cos\psi = s'b/\sqrt{a^2 + b^2}, \quad (10)$$

with $s, s' = \pm 1$. After a long, but straightforward, derivation we arrive at the following solution of Eq. (8) for the final energy as a function of the parameter σ

$$\frac{E_\mathbf{p}}{2\,U_p} = \frac{b^2}{a^2 + b^2}\left(2c^2 + d \pm 2c\sqrt{c^2 + d}\right), \quad (11)$$

where $c = (\cos\sigma + a)\cos\theta$ and $d = b(\cos\sigma + 3a)/\sigma$. We have also used the fact that the solutions are real if $ss' = 1$.

The solutions [Eq. (11)] as functions of $\omega\tau = 2\sigma$ (τ is the "travel time" of the liberated electron) are presented in Fig. 2(a) (BS) and Fig. 2(b) (FS) for lab-frame scattering angles θ between 0° and 90°. Similar results were obtained in Refs. [18,25,26]. It is important that the cutoff energy for the forward-scattered solutions increases with increasing angle θ. For example, the cutoff energy for $\omega\tau \approx 10$ in Fig. 2(b) increases from $0.1\,U_p$ for $\theta = 0°$ to above $0.5\,U_p$ for $\theta = 90°$. Owing to the symmetry of the driving laser field these curves are the same if we replace $\theta \to 180° - \theta$. Inspection of Figs. 2(a) and 2(b) shows that all curves except $\theta = 0°$ suddenly terminate at some points in the $(E_\mathbf{p}, \omega\tau)$ plane. Closer inspection confirms that a curve that terminates in Fig. 2(a) smoothly continues in Fig. 2(b) and vice versa so that a closed curve results if the two are taken together. This is a consequence of our notation of BS and FS solutions. Also note that some scattering angles are inaccessible for certain ranges of travel times.

If the electron revisits at times when the vector potential vanishes, no additional longitudinal drift momentum will be imparted and the electron rescatters isotropically with the kinetic energy with which it returned. This can be seen in Fig. 2 at $\omega\tau = 2.33$ [and again at larger values $\omega\tau = 9.21, 15.58, \ldots$, which are given by the solutions of $2\sigma\cos\sigma = \sin\sigma$ such that $c = 0$ in Eq. (11)], where the

curves for all angles θ intersect in one point, which specifies the energy $E_{\mathbf{p}} \approx 1.05\,U_p$.

In the upper panel of Fig. 3 we present the results obtained from the coherent sum of FS quantum-orbit contributions with $\mu \geq 1$. The pattern of nested diamonds (rhombi) of Fig. 3 in Ref. [25] is still visible, but has rich structures superimposed. Along the $p_\parallel$ axis, the first two LES energies stand out, which according to the soft-recollision model are located at the energies of $0.09438\,U_p$ ($p = 0.3676$ a.u.) and $0.03296\,U_p$ ($p = 0.2173$ a.u.)[18,22]. Away from the $p_\parallel$ axis, one recognizes the first two ATI rings with $p = 0.2136$ and 0.3020 a.u. corresponding to net absorption of 52 and 53 photons, respectively. Farther along the transverse axis, the cutoffs for 90° emission at $0.55\,U_p$ and $0.33\,U_p$ from Fig. 2 are visible. In addition there is a carpet-like pattern, which is generated by interference of different FS orbits. In the lower panel of Fig. 3 we present the coherent sum of both BS and FS quantum-orbit contributions. The three prongs of the fork-like structure of the off-axis LES[25] are clearly visible.

Next, in Fig. 4 spectra for particular values of the FS solutions μ are displayed. In the upper panel we compare the spectra for $\mu = 0$ obtained using the ISFA ($p_y < 0$) and the LFA ($p_y > 0$). Both spectra exhibit the characteristic diamond-like structure, but the LFA spectra are enhanced for small values of the momenta and the angle θ due to the large differential Coulomb cross section. Similar results hold for other values of μ (an example for $\mu = 8$ is shown in the lower panel of Fig. 4; the cutoff for $\mu = 8$ is much lower[18]). Note that the rich structure displayed in the upper panel of Fig. 3 (which is the superposition of several FS orbits) is absent in the contribution of just one FS orbit, which suggests that it is due to interference.

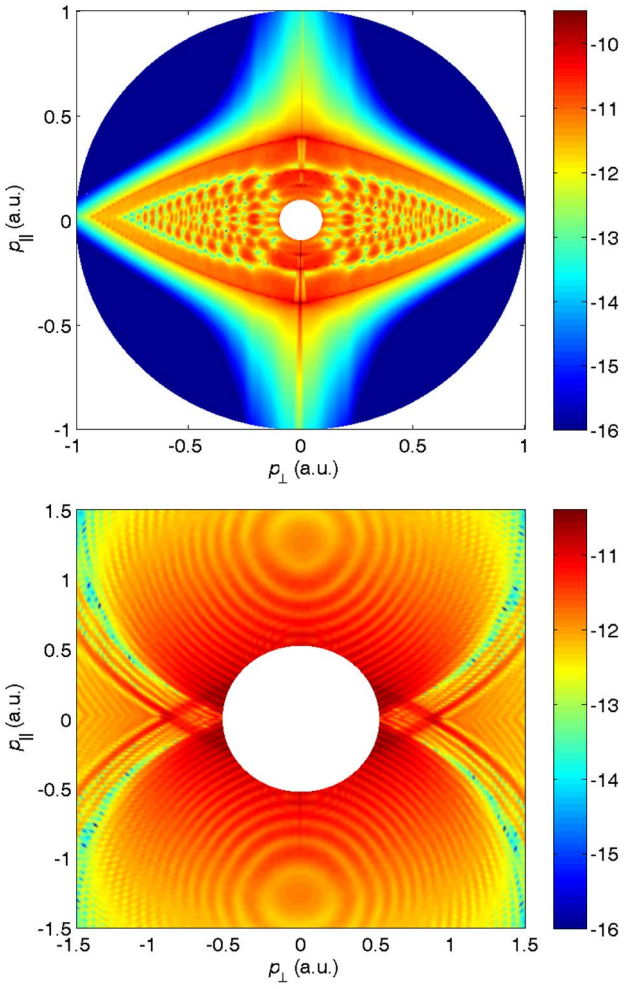

Fig. 3. Logarithm of the differential ionization rate of Xe presented in false colors (the color map covers more than 4 orders of magnitude in arbitrary units) in the electron momentum plane for ionization by a linearly polarized laser field with intensity $5.217 \times 10^{13}\,\mathrm{W/cm^2}$ and wavelength 2000 nm ($U_p = 19.49$ eV). Results are obtained using the coherent sum of forward-like scattering solutions with $\mu \geq 1$ (upper panel) and both of the forward-like and backward-like scattering solutions (lower panel).

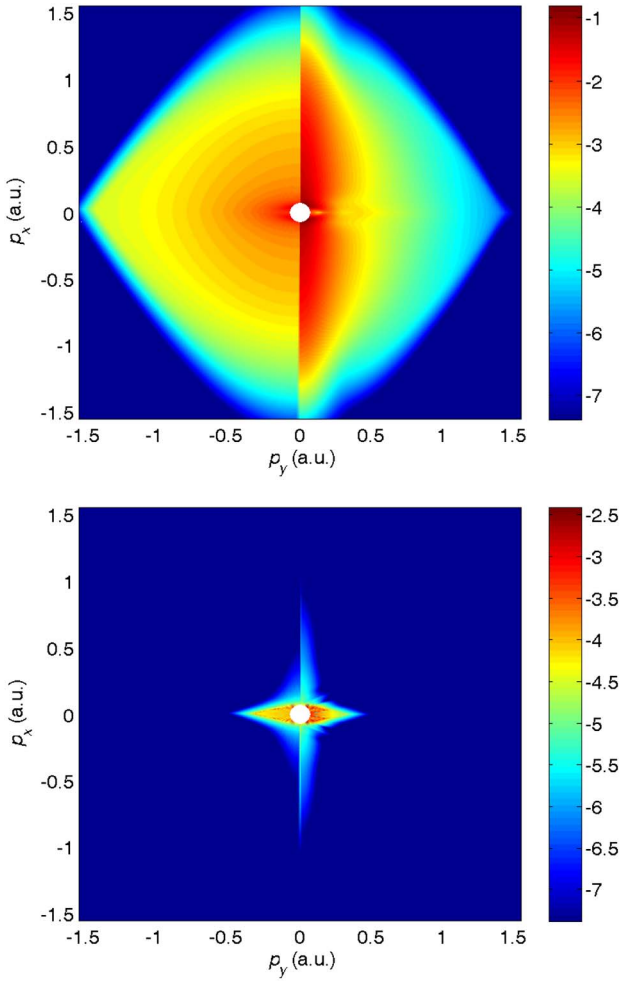

Fig. 4. Logarithm of the differential ionization rate of Xe presented in false colors in the electron momentum plane for ionization by a linearly polarized laser field having the intensity 4.5×10^{13} W/cm^2 and the wavelength 1800 nm ($U_p = 13.6$ eV). The upper (lower) panel exhibits the results obtained for the FS contribution $\mu = 0$ ($\mu = 8$). Rescattering matrix element is taken in the LFA (ISFA) for the right (left) part of each panel.

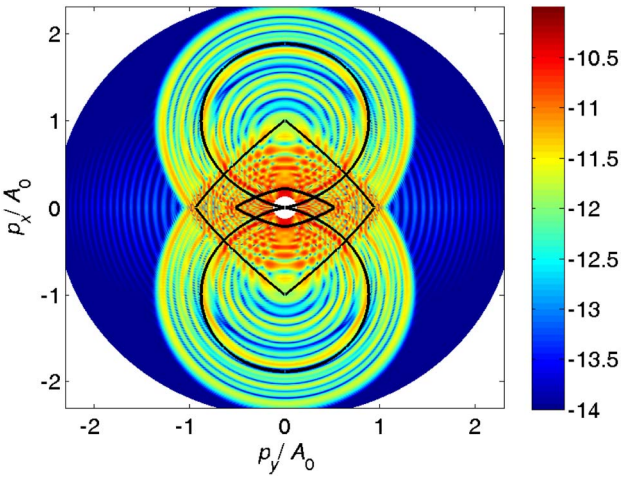

Fig. 5. Logarithm of the differential ionization rate of Xe, for the same laser parameters as in Fig. 4, presented in false colors in the electron momentum plane with the momentum expressed in units of the laser field vector potential amplitude A_0. Results are obtained using the ISFA with only the rescattering amplitude and numerical integration. Classical cutoffs of the electron drift energy, calculated by the method used in Ref. [25], for some characteristic orbits are represented by black lines. They can be compared with the cutoffs inferred from Fig. 2.

Figure 5 shows the ionization rate for Xe as calculated from only the rescattering amplitude within the ISFA. The black lines trace out the cutoffs of some FS orbits and are based on Ref. [25]; see also Fig. 2. The orbits that intersect at the origin will form the "V" structure recently observed at 3100 nm[27]. This will be discussed elsewhere. The ring structure at higher energies is partly due to the cutoffs of the longer BS orbits and partly due to their interference.

In conclusion, we collect various results regarding the quantum-orbit strong-field-approximation description of ATI into states with low electron-energy by intense mid-infrared fields. For the ionization of neutral atoms where the liberated electron is subject to the ion's Coulomb field forward rescattering makes important if not dominant contributions to the total ionization rate. This explains the LES as well as other off-axis structures that have been recently observed. We compare different approximations to the rescattering process and the relative significance of direct and (forward and backward) rescattered electrons. It seems that a unified description of ATI in terms of quantum orbits is emerging.

References

1. P. B. Corkum, Phys. Rev. Lett. **71**, 1994 (1993).
2. G. G. Paulus, W. Becker, W. Nicklich, and H. Walther, J. Phys. B **27**, L703 (1994).
3. G. G. Paulus, W. Nicklich, H. Xu, P. Lambropoulos, and H. Walther, Phys. Rev. Lett. **72**, 2851 (1994).
4. F. H. M. Faisal, Nat. Phys. **5**, 319 (2009).
5. C. I. Blaga, F. Catoire, P. Colosimo, G. G. Paulus, H. G. Muller, P. Agostini, and L. F. DiMauro, Nat. Phys. **5**, 335 (2009).
6. W. Quan, Z. Lin, M. Wu, H. Kang, H. Liu, X. Liu, J. Chen, J. Liu, X. T. He, S. G. Chen, H. Xiong, L. Guo, H. Xu, Y. Fu, Y. Cheng, and Z. Z. Xu, Phys. Rev. Lett. **103**, 093001 (2009).
7. E. Hasović, M. Busuladžić, A. Gazibegović-Busuladžić, D. B. Milošević, and W. Becker, Laser Phys. **17**, 376 (2007).
8. D. B. Milošević, E. Hasović, M. Busuladžić, A. Gazibegović-Busuladžić, and W. Becker, Phys. Rev. A **76**, 053410 (2007).
9. E. Hasović, A. Kramo, and D. B. Milošević, Eur. Phys. J. Sp. Top. **160**, 205 (2008).
10. A. Čerkić, E. Hasović, D. B. Milošević, and W. Becker, Phys. Rev. A **79**, 033413 (2009).
11. D. B. Milošević, A. Čerkić, B. Fetić, E. Hasović, and W. Becker, Laser Phys. **20**, 573 (2010).
12. D. B. Milošević, W. Becker, M. Okunishi, G. Prümper, K. Shimada, and K. Ueda, J. Phys. B **43**, 015401 (2010).
13. A. Čerkić, M. Busuladžić, E. Hasović, A. Gazibegović-Busuladžić, W. Becker, and D. B. Milošević, Phys. Scr. T **149**, 014043 (2012).
14. L. Guo, S. S. Han, X. Liu, Y. Cheng, Z. Z. Xu, J. Fan, J. Chen, S. G. Chen, W. Becker, C. I. Blaga, A. D. DiChiara, E. Sistrunk, P. Agostini, and L. F. DiMauro, Phys. Rev. Lett. **110**, 013001 (2013).
15. D. B. Milošević, Phys. Rev. A **88**, 023417 (2013).
16. D. B. Milošević, Phys. Rev. A **90**, 063414 (2014).
17. D. B. Milošević, Phys. Rev. A **90**, 063423 (2014).
18. W. Becker, S. P. Goreslavski, D. B. Milošević, and G. G. Paulus, J. Phys. B **47**, 204022 (2014).
19. C. F. de Morisson Faria, H. Schomerus, and W. Becker, Phys. Rev. A **66**, 043413 (2002).
20. D. B. Milošević and W. Becker, Phys. Rev. A **66**, 063417 (2002).
21. A. Čerkić and D. B. Milošević, Phys. Rev. A **73**, 033413 (2006).
22. A. Kästner, U. Saalmann, and J. M. Rost, Phys. Rev. Lett. **108**, 033201 (2012).
23. W. Becker, F. Grasbon, R. Kopold, D. B. Milošević, G. G. Paulus, and H. Walther, Adv. At. Mol. Opt. Phys. **48**, 35 (2002).
24. D. B. Milošević, G. G. Paulus, D. Bauer, and W. Becker, J. Phys. B **39**, R203 (2006).
25. M. Möller, F. Meyer, A. M. Sayler, G. G. Paulus, M. F. Kling, B. E. Schmidt, W. Becker, and D. B. Milošević, Phys. Rev. A **90**, 023412 (2014).
26. R. Kopold, "Atomare Ionisationsdynamik in Starken Laserfeldern," Ph.D. dissertation (Technische Universität München, 2001).
27. B. Wolter, C. Lemell, M. Baudisch, M. G. Pullen, X. M. Tong, M. Hemmer, A. Senftleben, C. D. Schröter, J. Ullrich, R. Moshammer, J. Biegert, and J. Burgdörfer, Phys. Rev. A **90**, 063424 (2014).